Taylor & Francis
Taylor & Francis Group

Vehicle System Dynamics
International Journal of Vehicle Mechanics and Mobility

ISSN: (Print) (Online) Journal homepage: https://www.tandfonline.com/loi/nvsd20

Reducing wheel–rail surface damage by incorporating hydraulic damping in the Bogie primary suspension

C. Qu, Y. Li, J.Z. Jiang, G.J. Tucker, S.A. Neild, M.C. Smith, A. Gleeson, S. Odetunde & Y. Muhamedsalih

To cite this article: C. Qu, Y. Li, J.Z. Jiang, G.J. Tucker, S.A. Neild, M.C. Smith, A. Gleeson, S. Odetunde & Y. Muhamedsalih (2022): Reducing wheel–rail surface damage by incorporating hydraulic damping in the Bogie primary suspension, Vehicle System Dynamics, DOI: 10.1080/00423114.2022.2092012

To link to this article: https://doi.org/10.1080/00423114.2022.2092012

Published online: 06 Jul 2022.

VEHICLE SYSTEM DYNAMICS
https://doi.org/10.1080/00423114.2022.2092012

Reducing wheel–rail surface damage by incorporating hydraulic damping in the Bogie primary suspension

C. Qu[a], Y. Li [a], J.Z. Jiang[a], G.J. Tucker[b], S.A. Neild[a], M.C. Smith[c], A. Gleeson[d], S. Odetunde[d] and Y. Muhamedsalih[b]

[a]Faculty of Engineering, University of Bristol, Bristol, UK; [b]Institute of Railway Research, University of Huddersfield, Huddersfield, UK; [c]Department of Engineering, University of Cambridge, Cambridge, UK; [d]RSSB, London, UK

ABSTRACT

Wheel–rail surface damage in curves can be effectively reduced with a lower vehicle Primary Yaw Stiffness (PYS), while lowering PYS is detrimental to ride comfort and vehicle stability. This trade-off can be addressed by integrating hydraulic damping into primary suspension. However, work in this area only concentrated on comparing the effects of specific devices – the full potential of the hydraulic-damping-integrated primary suspension on combating the trade-off considering the whole parameter space is still unknown. Here we address this by making the following two contributions: (1) fully exploring the potential of hydraulic-damping-integrated primary suspension, on minimising the PYS while maintaining ride comfort; (2) systematically investigating the trade-off between the PYS reduction and suspension stroke requirement. Based on a case study using the Mark 4 Coach, this paper found that the optimal hydraulic-damping-integrated suspension can reduce PYS by 97% over the default without worsening comfort. This large reduction can potentially lead to a significant lifetime wheel-rail maintenance cost saving of approximately £42M for the fleet. If a larger suspension stroke is allowed, more cost saving can be achieved. These results provide motivation to conduct detailed engineering design studies to further examine the trade-off between financial benefits and design complexity.

ARTICLE HISTORY
Received 21 March 2022
Revised 23 May 2022
Accepted 11 June 2022

KEYWORDS
Railway vehicle; wheel and rail surface damage; passive absorber; hydraulic damping; primary suspension

1. Introduction

Maintaining wheels and rails to manage surface damage represent a significant proportion of the maintenance cost of the railway system. The frictional energy loss due to the wheel and rail tangential force and the creepage at the contact patch lead to the surface damage, especially during curved sections. Research attention has been made to achieve reduced wheel–rail surface damage using both active and passive control methods. For example, passive control methods include optimising the wheel profile [1], introducing the linkage bogies to the steering locomotive [2], optimising vehicle suspensions [3], and

CONTACT Y. Li yuan.li@bristol.ac.uk

the geometric and inertial parameters [4]. Active methods have also been investigated, such as introducing independent-rotating-wheel systems where a wheelset angle of attack feedback controller is used [5–7]. Among these solutions, design of vehicle suspension components using passive methods are regarded as an attractive approach because of their design simplicity, cost-effectiveness and reliability [8].

In the previous research, designs of primary suspensions to minimise the wheel–rail surface damage have drawn lots of attention. The studies in [9–11] have shown that with a decrease in the longitudinal static stiffness of the primary suspension, the rail surface damage can be significantly reduced. This is because the longitudinal primary-suspension static stiffness plays a significant role in the vehicle primary yaw stiffness (PYS) – a smaller longitudinal primary stiffness, a lower PYS. A lower PYS results in a reduced resistance to yaw motion between bogie and wheelset, allowing better radial alignment of wheelsets during curving. This in turn reduces the frictional energy loss at the contact patch and therefore contribute to less rail surface damage [8]. However, decreasing the PYS may cause the vehicle to react more strongly to track geometry irregularities, leading to higher levels of lateral carbody acceleration, thus worsening passengers' ride comfort. Besides, at higher speeds, a vehicle with a reduced PYS tends to have an unstable response to track geometry irregularities, in the form of bogie 'hunting'. Such bogie hunting happens above a 'critical speed', which is directly dependent on the PYS [12] (generally a lower PYS leads to a lower critical speed). This unstable phenomenon may increase the risk of derailment, which is problematic from a safety perspective [13–16]. Therefore, in order to provide sufficient reduction in surface damage, the vehicle is required to have a smaller PYS; to achieve satisfactory ride comfort and stability performance, a large PYS is desirable. Then for the primary suspension, it is required to achieve both small longitudinal static stiffness which would result in lower levels of surface damage in curves and large high-frequency longitudinal dynamic stiffness for satisfactory ride comfort and stability performance.

Conventional passenger vehicle bogies use the trailing arm suspensions incorporating rubber bushes, to connect the pivot of the trailing arm to the bogie [17–19]. These rubber bushes can provide stiffness and a limited level of damping in different directions. These properties cannot provide the desirable frequency-dependent dynamic performance, i.e. low longitudinal static stiffness while large high-frequency dynamic stiffness. Alternative to rubber bush, a hydraulic damped bush, the HALL® bush, is starting to be used on some railway vehicles as part of the primary suspension. As reported in [20], the HALL ® bush has the desirable characteristics of a low static stiffness and a high dynamic stiffness at high frequencies. Such frequency-dependent dynamic behaviour is achieved through the introduction of hydraulic damping. Results in [20] have shown that this HALL® bush can efficiently reduce rail surface damage in curves whilst maintaining the vehicle stability performance.

Despite the benefits achieved, it should be noted that the work in [20] only concentrated on introducing the effect of a specific hydraulic-damping-integrated device (with a specific parameter setting) on addressing the trade-off between surface damage and vehicle stability performance. There is no study exploring the full stiffness-damping parameter space. Because of this, the potential of minimising vehicle PYS, hence minimising surface damage in curves, using primary suspension incorporating hydraulic damping has not been fully explored. Suspension stroke is an important factor affecting suspension packaging [21]. It is anticipated that primary suspension stroke in both longitudinal and lateral directions

will be affected with a reduced PYS. However, to date, it is still unclear how the suspension stroke requirement affects the achievable PYS reduction, hence wheel–rail surface damage reduction. This work fills the gaps and makes twofold contribution: (1) to fully explore the potential of integrating hydraulic damping into primary suspension, on minimising the PYS while not compromising ride comfort and stability performance. (2) To thoroughly investigate the trade-off between the allowable primary suspension stroke and the achievable PYS reduction. In addition, a high-level business case has been provided to demonstrate the potential lifetime cost saving achieved by the new suspension designs over the conventional and HALL® bushes. The resultant cost saving with different levels of PYS reduction and suspension stroke requirements are estimated and compared. It is worth noting that the investigation carried out in this work would give rail engineers practical guidance on primary suspension design with hydraulic damping integrated, and provide motivation to conduct detailed engineering design studies to further examine the trade-off between financial benefits and design complexity.

This paper is structured as follows. Section 2 introduces the vehicle model adopted in this paper. The conventional rubber bush and a specific HALL® bush used in the vehicle primary suspension are also introduced. Section 3 details the optimal design of the primary suspension with hydraulic damping integrated, to minimise the vehicle PYS while satisfying the ride comfort performance constraint. The vehicle stability performance with the optimum design has also been investigated. Section 4 investigates the wheelset and suspension performance during two curving cases with the optimised designs. Section 5 introduces a further optimisation, investigating the trade-off between the maximum suspension stroke and the PYS reduction. The total cost saving for the Mark 4 fleet incorporating optimised hydraulic-integrated primary suspensions with different stroke constraints have been compared. Finally, conclusions are obtained in Section 6.

2. Vehicle model

In this Section, the vehicle model considered in this work is introduced. The parameters of the baseline primary suspensions with the default rubber bush and the hydraulic-damping-integrated bush (HALL® bush) are presented, as well as their resulting PYS.

2.1. Model description

This work considers a four-axle two-bogie vehicle with a trailing arm bogie suspension arrangement, Mark 4 Coach. This is a typical vehicle used in intercity operations on the GB mainline network with a speed of up to 125 mph (55.5 m/s). Simulations have been carried out using a commercial multi-body dynamics software, VAMPIRE®. A vehicle model from the Vehicle Track Interaction Strategic Model (VTISM) [22], the 'BogiePassenger_45t_40yaw.veh'[1], has been selected since as suggested by the VTISM library, it is broadly representative of a Mark 4 Coach. It is worth noting that the Mark 4 Coach has already been retrofitted with a HALL® bush and the bush properties have been given in [20]. However, as mentioned in the Introduction section, this retrofitted HALL® bush has a specific parameter setting, while this research seeks to fully explore the performance potential provided by hydraulic-damping-integrated bush through systematical optimisation. A 3D view of the vehicle model with two bogies has been shown

in Figure 1(a). As the current work focuses on optimising primary suspension, a plan view for one of the bogies is also presented in Figure 1(b), where only the primary suspension components that act in the horizontal plane are shown (longitudinal X, lateral Y and yaw W directions). The primary suspension on a Mark 4 Coach consists of a trailing arm bush, a primary vertical spring and a primary vertical damper, the contribution of the trailing arm bush along each direction can be modelled as a static spring in parallel with a

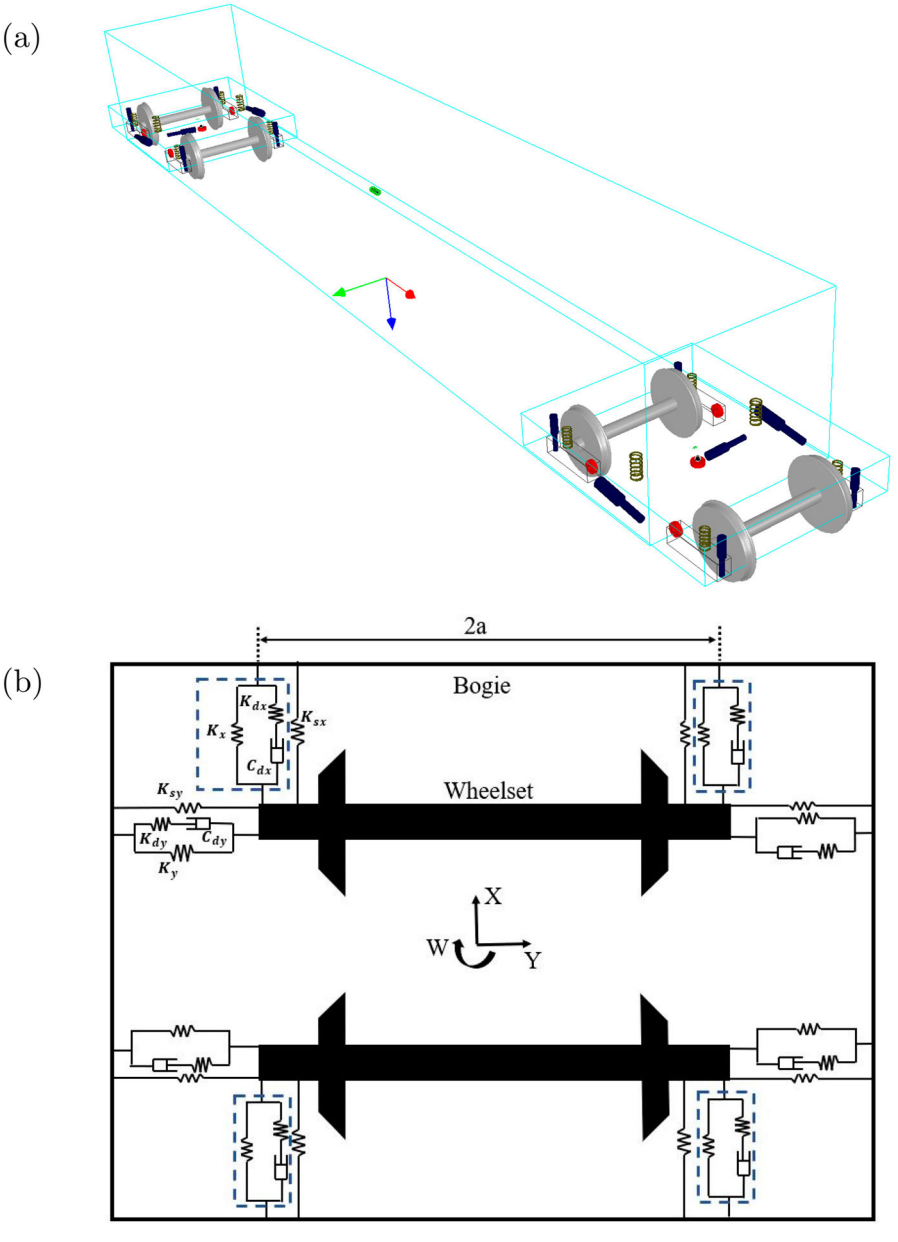

Figure 1. (a) 3D view of the considered vehicle model in VAMPIRE® and (b) the schematic plot of the two-axle bogie in the horizontal plane (longitudinal X, lateral Y and yaw W direction).

Table 1. Vehicle primary suspension components and symbols.

Symbol	Suspension component
K_x	Longitudinal static stiffness from trailing arm bush
K_{dx}	Longitudinal dynamic stiffness from trailing arm bush
C_{dx}	Longitudinal damping from trailing arm bush
K_{sx}	Longitudinal shear stiffness from vertical spring
K_y	Lateral static stiffness from trailing arm bush
K_{dy}	Lateral dynamic stiffness from trailing arm bush
C_{dy}	Lateral damping from trailing arm bush
K_{sy}	Lateral shear stiffness from vertical spring

series spring-damper. A list of the vehicle bogie suspension components with their relevant parameter symbols is provided in Table 1.

The total PYS of the Mark 4 Coach can be written as

$$\text{PYS} = 2a(K_x + K_{sx}) \tag{1}$$

where $a(=1\text{ m})$ represents the semi-lateral spacing between the left and right trailing arm bushes for each bogie, K_x is the longitudinal static stiffness of the trailing arm bush and K_{sx} is the primary vertical spring acting in shear. For the chosen passenger vehicle, the total PYS is 40 MNm/rad with single K_{sx} equals to 0.57 MN/m and single K_x equals to 19.43 MN/m. It can be seen that the main contribution to the PYS comes from the static stiffness of the trailing arm bush in the longitudinal direction, K_x, and any reduction in K_x will decrease the PYS. Therefore, in the following optimisation, the longitudinal static stiffness of the trailing arm bush, K_x, will be used as the cost function to be minimised (the vertical spring is kept at its default value).

2.2. Default rubber, HALL® and optimised hydraulic bushes

Table 2 shows the comparison of the parameter sets for the default Mark 4 rubber bush, denoted as S_{DR} ('DR' stands for default rubber), and the specific hydraulic-damping-integrated bush, HALL® bush [20], in the longitudinal direction. As introduced in Section 1, the conventional rubber bush cannot provide sufficient reduction in wheel–rail surface damage in curves and maintain the ride comfort and stability performance simultaneously. With the introduction of hydraulic damping into the rubber bush, a significant reduction in surface damage can be achieved without worsening the ride comfort performance. This is because the new design of the bush contains fluid chambers and a fluid passageway. As the fluid in the device being compressed through the fluid passageway, the damping force attributing to the fluid resistance is significantly larger than the rubber damping and allows frequency-dependent behaviour [20]. With the integrated hydraulic damping, a low quasi-static stiffness during curves and a high dynamic stiffness at high frequency is possible. In addition, the parameter range for hydraulic damping can be broadened by switching the fluid type and modifying the dimension of the fluid passageway. From Table 2, it can be seen that, with the introduction of the hydraulic damping (up to 6563 kNs/m) and a significantly reduced K_x (3.9 MN/m), the total PYS can be reduced by up to 78% compared with using the default bush S_{DR}. These parameters are from the work in [20], while it only introduced a specific example of the hydraulic bush. The potential

Table 2. Parameter values for the default rubber bush, S_{DR}, the HALL® and the optimised hydraulic bush S_{OH}, in the longitudinal direction.

Configuration	K_x (MN/m)	K_{dx} (MN/m)	C_{dx} (kNs/m)	Total PYS (MNm/rad)	PYS reduction (%)
Default Rubber Bush – S_{DR}	19.43	38.86	19.43	40.00	–
Default HALL® Bush	3.90	25.00	6563.00	8.94	77.7
Optimised Hydraulic Bush – S_{OH}	0.00	16.42	6686.00	1.14	97.2

of maximising the achievable PYS reduction with the primary suspension incorporating hydraulic damping has not been fully explored. The following section will therefore present a systematic optimisation to a general hydraulic system setting for the longitudinal trailing arm bush. Note that the S_{OH} ('OH' stands for optimised hydraulic) in Table 2 refers to the optimised hydraulic-damping-integrated bush in longitudinal direction, which will be introduced in Section 3.

2.3. Wheel–rail contact modelling

The methods used for modelling the wheel–rail contact are important, as they significantly affect the simulated vehicle dynamic performance. Railway wheelsets are designed with coned wheels, which create the rolling radius difference (RRD) that naturally steers the wheelset back towards the track centre line. The RRD achieved with coned wheels is an important feature in negotiating curves. When the RRD steers a wheelset back towards the centre line of the track, the wheelset can overshoot and hence set up an oscillatory motion which could lead to vehicle instability, if there is inadequate damping. In practice, wheel profiles are not pure cones, but are designed with specific profile shapes in order to improve their dynamic behaviours through the track. Therefore, an 'equivalent conicity' has been introduced to give an indication of how RRD changes with lateral displacement [23]. The equivalent conicity can also be affected by the wheel worn condition, typically increasing over its life cycle, therefore, the suspensions need to work effectively both with new and worn wheels (see detailed explanation in Appendix 1). In this work, the constant equivalent conicities ranging from 0.1 to 0.5 are considered, in order to establish a realistic simulation case covering the wheel profile with different worn conditions.

During the optimisation procedure, square root creep law is selected for wheel–rail contact modelling, to calculate the creepages (relative velocities) and the resulting creep forces generated at the wheel–rail contact. This is because of its unique advantages: (1) compared with the model using nonlinear creep law (i.e. the realistic nonlinear relationship between creepage and creep force is considered), square-root-creep law is more computationally efficient; (2) compared with the pure linear creep law, square-root-creep law is more precise because it considers the creep force saturation nonlinearity and flange contact nonlinearity. However, it should be noted that the more detailed nonlinear contact model is used for performance assessment after the optimisation in Section 4 in order to obtain more accurate vehicle's dynamic performance. The equivalent conicity of the nonlinear wheel–rail contact data are measured when the wheelset has a relative displacement of 3 mm based on UK standard. In addition, the fully nonlinear friction saturation with a coefficient of friction value of 0.32 is used based on [8].

3. Optimisation minimising PYS

In this section, the systematic optimisation of the primary trailing arm bush integrated with hydraulic damping is presented, to fully explore its potential on wheel–rail surface damage reduction. The optimisation procedure, including the cost function and performance constraints, is introduced, and the optimisation results are presented. An assessment of the resulting stability performance achieved by the optimal design is carried out, in comparison with the baseline cases.

3.1. Design problem formulation and baseline performance

In this work, the longitudinal component of the trailing arm bush is optimised. The target of the optimal design problem is to reduce the longitudinal static stiffness of the trailing arm bush, K_x, which is the main contribution to the PYS, see Equation (1). The parameters in the longitudinal component of the trailing arm bush are optimised while the lateral and vertical component parameters are kept as the default. For the existing hydraulic-damping-integrated bush, the effective damping is achieved by fluid being compressed through the fluid passageway. The damping value could reach to a level of 7000 kNs/m, based on initial calculation considering the fluid properties and the dimension of fluid passageway [24]. Hence, in the following optimisation of the general hydraulic bush, a limit of 7000 kNs/m is imposed on the damping value, while the stiffness is capped at 50 MN/m, matching the conventional rubber bush. Note that the hydraulic damping range in this study is only an estimation, a more accurate damping range can only be identified via detailed physical realisation considerations (which is beyond the scope of this study).

When K_x is reduced, the total vehicle's PYS is also reduced. Then, it is necessary to make sure that the passenger's ride comfort and stability performance should not be compromised. In this work, the passenger ride comfort of the vehicle is set as the optimisation constraint. The Root Mean Square (RMS) of the carbody lateral acceleration[2] is selected to represent the level of ride comfort and is compared with the default vehicle performance. A straight track file from VAMPIRE® library – 'track200.dat' has been selected to represent a typical GB track with line speed of 200 kph (55.6 m/s). In order to obtain a thorough analysis on the vehicle ride comfort performance during operation, different speeds and wheel concities have been considered. Here, combined operation conditions of three different speeds (33.3, 44.4, 55.6 m/s) and three contact conicities (0.1, 0.3, 0.5), forming a total of nine cases, are considered. Note that the RMS lateral acceleration at high speed and high conicity will inherently consider the vehicle stability performance. Therefore, the constraint based on stability is not directly used in the optimisation. However, a separate assessment of the vehicle stability performance is carried out in Section 3.3, using the design obtained from the optimisation.

Figure 2 shows the average RMS carbody lateral acceleration, measured above each bogie, for the vehicle travelling over the 'track200.dat' with the conventional rubber bush S_{DR} and the HALL® bush. As shown in the figure, the RMS accelerations representing ride comfort increase with speed and equivalent conicity. It has been illustrated that, compared with the S_{DR}, the vehicle with HALL® bush retrofitted provides slightly higher RMS accelerations in some operational cases, e.g. up to 5% at 55.6 m/s (see Figure 2(c)). Therefore, one of the ride comfort constraints for the optimisation is set as: at 55.6 m/s allowing

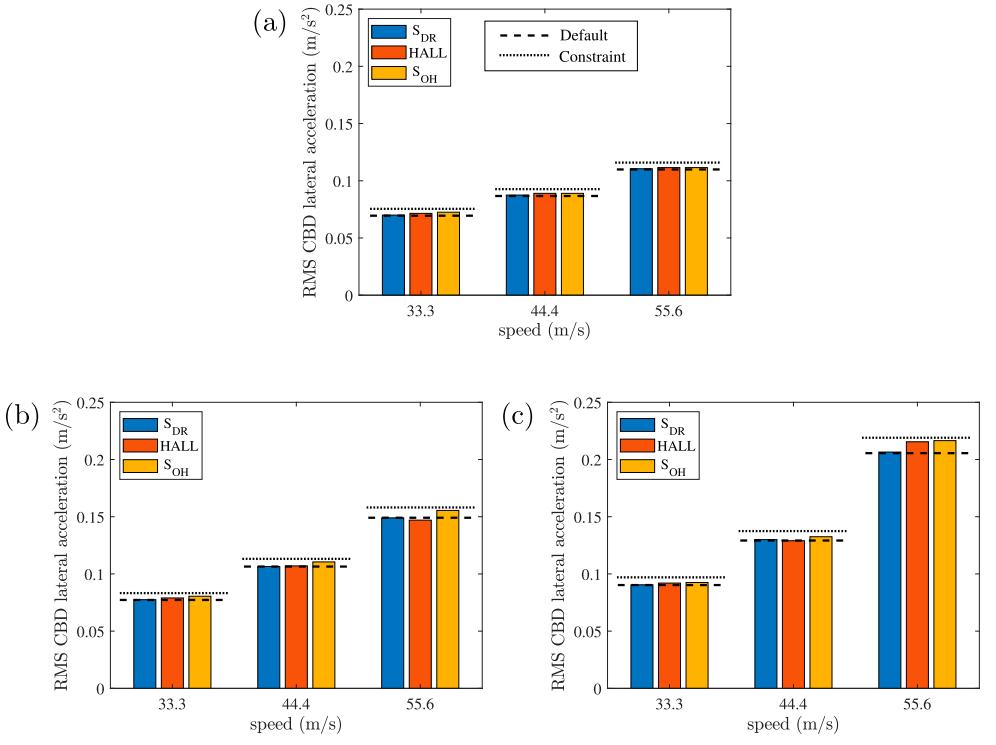

Figure 2. The ride comfort comparison in terms of RMS carbody lateral accelerations provided by the S_{DR}, the HALL® and S_{OH} at the equivalent conicity (a) 0.1, (b) 0.3 and (c) 0.5.

5% increase in the RMS of carbody lateral acceleration compared with the S_{DR}. At lower speeds, a 10% relaxation from the default levels is permitted, because these cases are less critical (with lower values of acceleration).

In summary, the longitudinal component of the trailing arm bush is optimised with the aim to minimise K_x. The parameter range of up to 7000 kNs/m for damping (C_{dx}) and up to 50 MN/m for the stiffness (K_{dx}) are considered. The ride comfort, quantified by the RMS of carbody lateral accelerations, is taken as constrains, where a 5% relaxation in the RMS acceleration over the default values are permitted at the highest speed (55.6 m/s), and 10% relaxation for the lower speeds. The co-optimisation has been carried out using the MATLAB® Optimisation Toolbox (Generic Algorithms such as Particle Swarm Optimisation) which assigns the suspension parameters and calls VAMPIRE® to simulate the vehicle dynamics and obtain the RMS accelerations. In each iteration, the suspension parameters are changed to find the optimal solution with the smallest K_x whilst maintaining the ride comfort constraints.

3.2. Optimisation results

Results of the optimisation show that the trailing arm bush using the default S_{DR} layout with a hydraulic damping could reduce the static longitudinal stiffness to zero. The parameter values for the optimised trailing arm bush (referred as 'S_{OH}') is given in Table 2. It

can be found the S_{OH} can provide a 97% PYS reduction compared with the default S_{DR} and around 87% PYS reduction compared with the HALL® bush. Note that since K_x has already been reduced to zero, the total PYS will only come from the longitudinal stiffness of the primary vertical spring acting in shear.

Figure 2 shows the comparison of ride comfort performance at different conicity and speed cases using nonlinear wheel–rail contact profile. It can be seen that the RMS carbody lateral acceleration provided by the optimised trailing arm bush, S_{OH}, with zero K_x, is still less than 5% at the worst case (which is within the constraints).

3.3. Stability assessment

As mentioned in Section 3.1, after the optimisation, a separate stability assessment is carried out using the suspension values derived from the optimisation procedure. For this analysis, the critical speed of all vehicle derivatives has been calculated based on a simulation process. This uses a VAMPIRE® library track, 'stability.dat', which includes a short (180 m) section of large lateral track irregularities to excite the lateral movement of the vehicle, followed by a straight and level track (820 m) with no irregularities. A vehicle is repeatedly simulated running on this track with increasing speed until reaching a critical speed where the suspension cannot effectively damp down the lateral oscillation induced at the start of the track and a limit cycle motion will be observed. An example of the limit cycle motion on the wheelset lateral acceleration has been given in Figure 3(a).

The identified critical speeds for different suspension configurations under equivalent conicities of 0.1, 0.3 and 0.5 have been compared in Figure 3(b). Note that the nonlinear wheel–rail contact model is used here. Across all three cases, the S_{OH} solution is found to provide similar critical speeds compared with the default rubber bush S_{DR} and the HALL® bush.

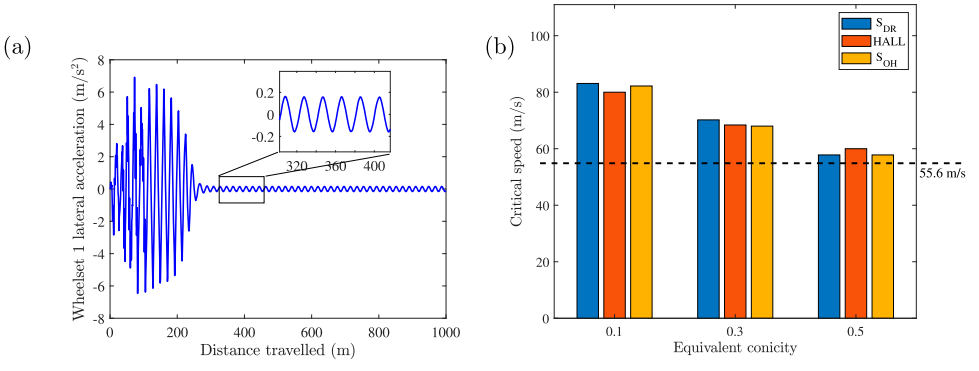

Figure 3. (a) An example of wheelset limit cycle motion and (b) the stability performance comparison in terms of the critical speed among S_{DR}, the HALL® and S_{OH}.

4. Curving performance with optimised suspension

In Section 3, the ride comfort and stability performance of the vehicle employing the optimal S_{OH} configuration have been assessed and no significant deterioration in their performance was found. Both performances were highly dependent on the suspension high dynamic stiffness at high frequencies, while the low static stiffness did not contribute significant effects to the performance. In this section, the effects of reducing K_x to zero on quasi-static curving will be assessed. Two curving scenarios are simulated in VAMPIRE®, one for the moderate curve with the radius equal to 1000 m, and the other for a tight curve with the radius equal to 200 m representing the most severe case. The wheelsets and suspensions performance with the S_{OH} configuration are assessed and compared with the default S_{DR} and the conventional HALL® bush. Besides, the maximum wheelset T_γ of three suspension configurations, which is a measure to quantify the wheel–rail surface damage [25], is also investigated and compared with the default and HALL® bush cases.

4.1. Wheelset performance

The vehicle wheelset performance with different primary suspensions (S_{DR}, the HALL® bush and S_{OH}) are assessed in this subsection. The track inputs for both moderate and tight curve scenarios have been given in Figure 4(a), where the tracks are straight for the first 100 m, followed by a 100 m curve transition, leading to a constant curve of either 200 m or 1000 m radius. Figure 4(b) shows the plan view of the two-axle bogie, where an example wheelset angle of attack (AOA, relative yaw angle to the track) and the wheelset lateral displacement have been illustrated. The vehicle is travelling to the positive direction, which is to the right of the paper and along the track which curves to the right. The positive lateral direction points to the downward of the paper and the positive yaw angle rotates in clockwise. The nonlinear contact model is used based on measured wheels and rails giving a 0.1 equivalent conicity (which is the most common scenario during operation, see Appendix 1).

Figure 5 shows the wheelset performance during the 1000-metre-radius curve, where the vehicle is operating at the balancing speed of 26 m/s with 100 mm applied cant. The

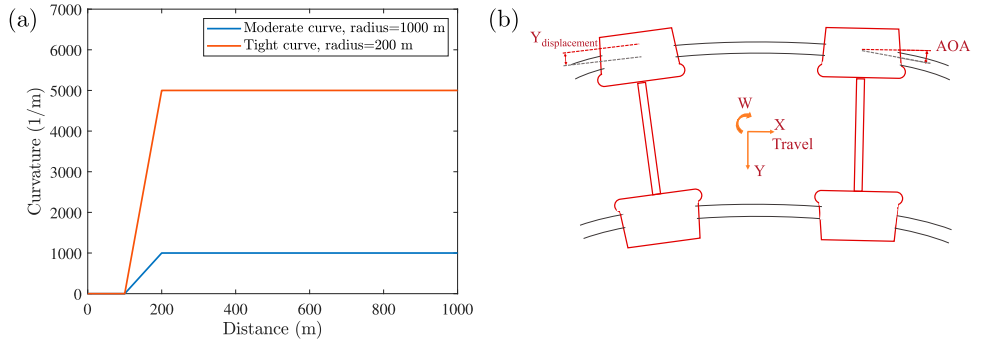

Figure 4. (a) The track inputs for the two curving scenarios. (b) Example strokes of the wheelsets from the leading bogie on curve, where the positive travelling direction points to the right of the paper, the positive lateral direction points to the downward of the paper and the positive yaw angle rotates in clockwise.

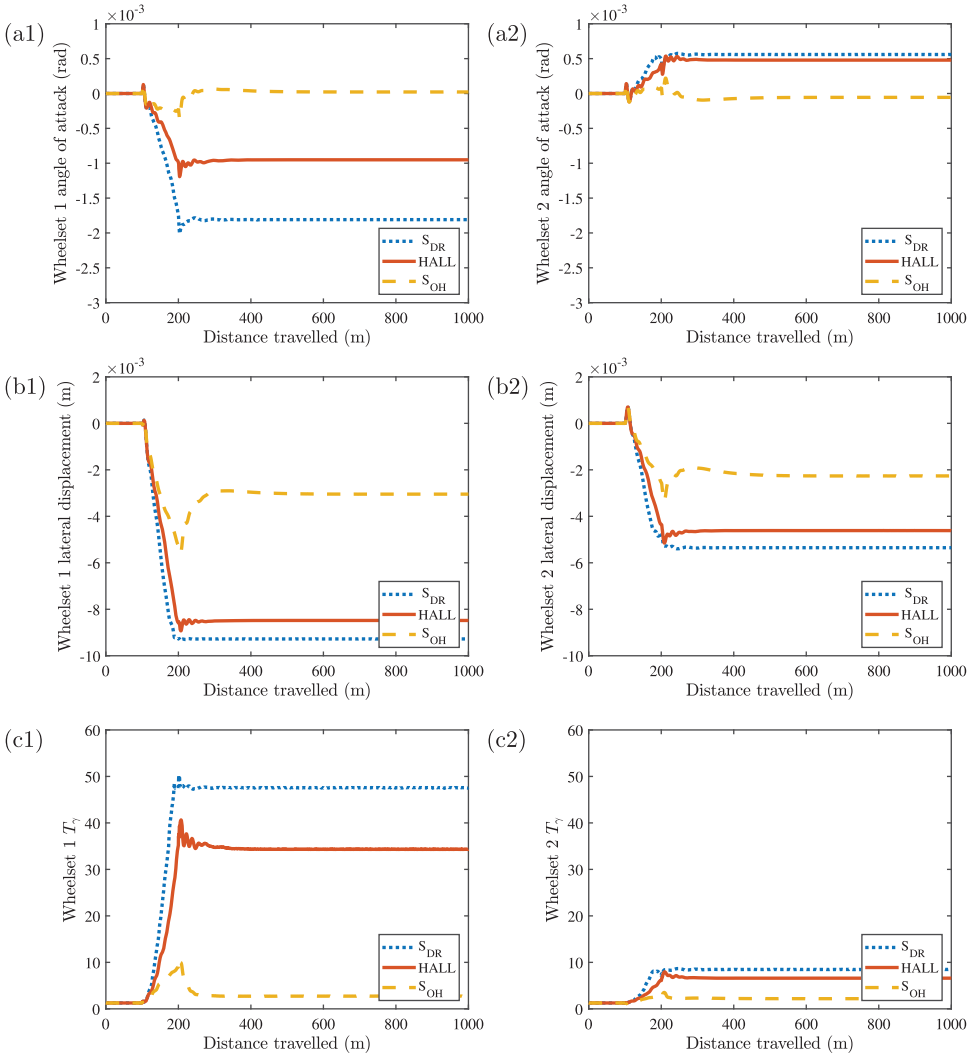

Figure 5. The wheelset performance comparison among S_{DR}, the HALL® and the S_{OH} during 1000-metre-radius curve, in terms of: (a1) and (a2) the angle of attack for wheelset 1 (leading wheelset) and wheelset 2 (trailing wheelset), (b1) and (b2) the wheelsets lateral displacements, (c1) and (c2) the wheelsets T_γ measured at the left wheel tread.

angle of attack of the leading wheelset (wheelset 1) and the trailing wheelset (wheelset 2) have been presented in Figure 5(a1) and (a2), respectively. It can be found that the vehicle with the S_{OH} suspension has a smaller angle of attack compared with those with the S_{DR} and the HALL® bush, showing better radial alignment due to the reduced PYS. Figure 5(b1) and (b2) shows the wheelset lateral displacement relative to the track, where smaller lateral displacement of the wheelsets has been found for the S_{OH} solution.

The wheelset T_γ of the S_{OH} has also been assessed, along with the default suspension and the HALL®. The T_γ is an important measure for the wheel–rail surface damage, and it has a direct relationship with the wheelset and track maintenance cost. The wheelset

T_γ is defined as the wheel–rail contact tangential force multiplied by wheel–rail contact tangential creepage, which can be expressed as:

$$T_\gamma = F_x c_x + F_y c_y + F_w c_w \tag{2}$$

Here F_x and F_y are the longitudinal and lateral creep forces between wheel and rail with unit of N, c_x and c_y are the corresponding creepage (without unit) and F_w (Nm) and c_w (rad/m) are the creep moment and creepage at spin direction, which are only computed for nonlinear simulations. Figure 5(c1) and (c2) shows the T_γ comparison for the vehicle with different primary suspensions. For this moderate curve case, the contact force and the surface damage mainly come from the tread contact between the rail and the left wheel for all vehicle derivatives (as the rail is curving to the right during the assessment, readers can refer to Appendix 2 for the details of wheel tread contact). So, the wheelset 1 and wheelset 2 T_γ measured at left wheel tread are compared , respectively, in Figure 5(c1) and (c2). It can be seen that as the angle of attack and the lateral displacement of the wheelsets being reduced with the optimised S_{OH} solution, a significant reduction on T_γ can be achieved compared with the default and the HALL®. This suggests less surface damage between the wheel and the rail will occur.

Apart from the moderate curve case, the tightest curve has also been considered here. The curve with 200-metre-radius and 100 mm applied cant is selected, and the vehicle is operating at the balancing speed of 12 m/s. The same wheel and rail contact profile has been used as the 1000-metre-radius curve case. The vehicle performance with the three suspension configurations have also been compared.

Figure 6(a1) and (a2) shows the wheelsets angle of attack comparison, where the bogie with S_{OH} solution has an overall better radial alignment and a significantly reduced angle of attack for the leading wheelset (wheelset 1), though a very small increase in angle of attack for the trailing wheelset (wheelset 2). Same situation occurs for the lateral displacement in Figure 6(b1) and (b2), where a larger relative lateral displacement to the track for wheelset 2 has been found with the S_{OH} configuration, while it is still smaller and within acceptable range if compared with the wheelset 1 in Figure 6(b1). During the tightest curve, the significant wheel–rail force will occur at the left wheel flange for wheelset 1 across all vehicle derivatives (see Appendix B). Therefore, the T_γ of the wheelset 1 measured at the left wheel flange has been compared in Figure 6(c1), where a significant reduction with S_{OH} solution could be found. However, for wheelset 2, the wheel–rail force occurs at the left wheel tread for the S_{DR} and the HALL® bush solutions, while for the S_{OH} solution the contact force occurs at the left wheel flange. So the T_γ of the wheelset 2 for S_{DR} and the HALL® bush are measured at left wheel tread, and for S_{OH} is measured at left wheel flange. These T_γ have been compared in Figure 6(c2). It can be found that the S_{OH} configuration has an overall reduced wheelset T_γ due to the reduced PYS, showing a significant reduction in energy loss.

In order to ensure a thorough analysis, a more detailed curving assessment considering the radius from 1000 m to 200 m with 100 m intervals have been carried out. The maximum left wheel T_γ among all wheelsets have been compared with different suspension configurations in Figure 7. For all the curving cases, the vehicle has been operated at a balancing speed with applied cant of 0.1 m. For the three suspensions, the maximum T_γ reduces when the curving radius increases, as the contact creep force and the creepage between wheel and rail become smaller. It is notable that the vehicle with S_{OH} suspension exhibits

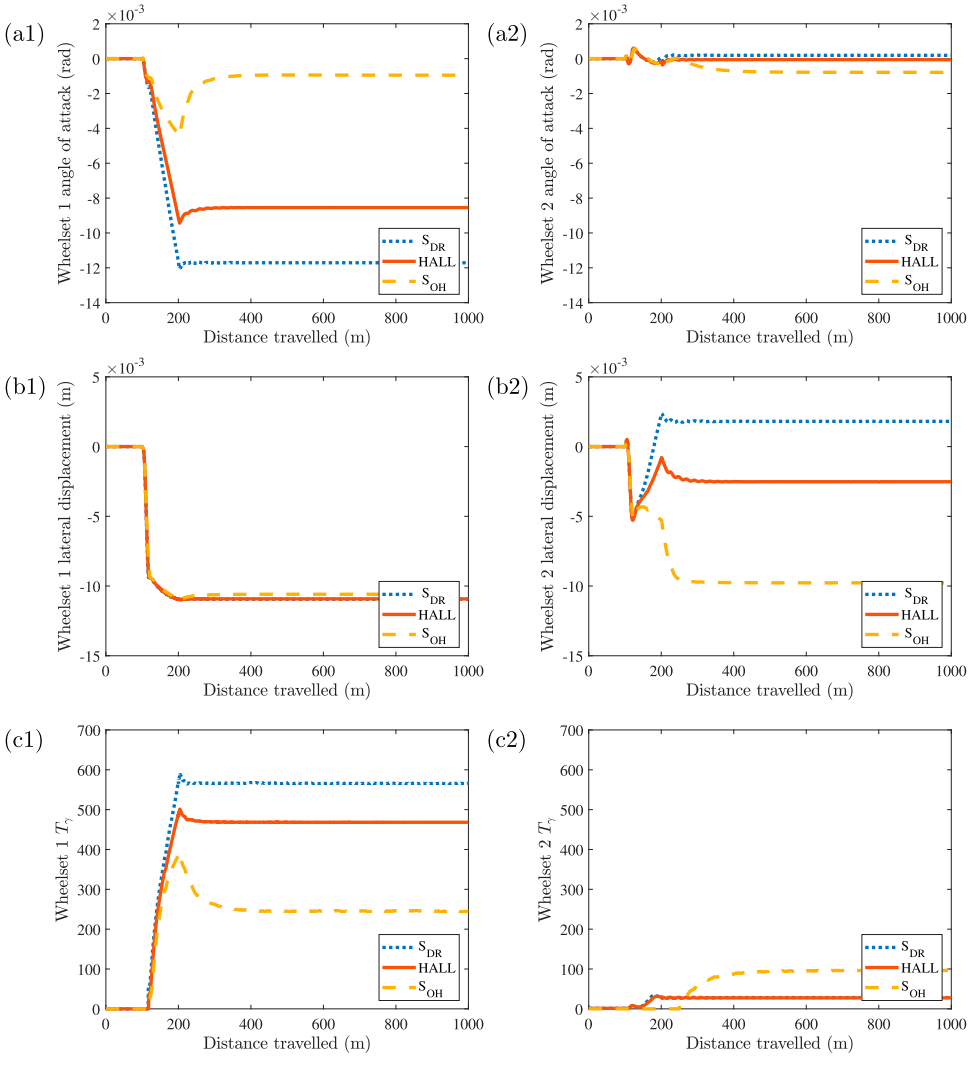

Figure 6. The wheelset performance comparison among S_{DR}, the HALL® and the S_{OH} during 200-metre-radius curve, in terms of: (a1) and (a2) the angle of attack for wheelset 1 (leading wheelset) and wheelset 2 (trailing wheelset), (b1) and (b2) the wheelsets lateral displacements, (c1) the wheelset 1 T_γ measured at left wheel flange and (c2) the wheelset 2 T_γ measured at left wheel tread for S_{DR} and the HALL® and left wheel flange for S_{OH}.

the smallest wheelset T_γ among all candidate suspensions and curving radius. Compared with the default S_{DR}, the vehicle with S_{OH} can provide a 40% reduction in wheelset T_γ in the 200 m-radius case and further reduction can be achieved as the curving radius becomes larger (80% for the 1000 m-radius case).

4.2. Suspension strokes

Apart from the wheelset performance during curving, the suspension strokes are also studied using the same curving scenarios introduced in Section 4.1. Here, the suspension stroke

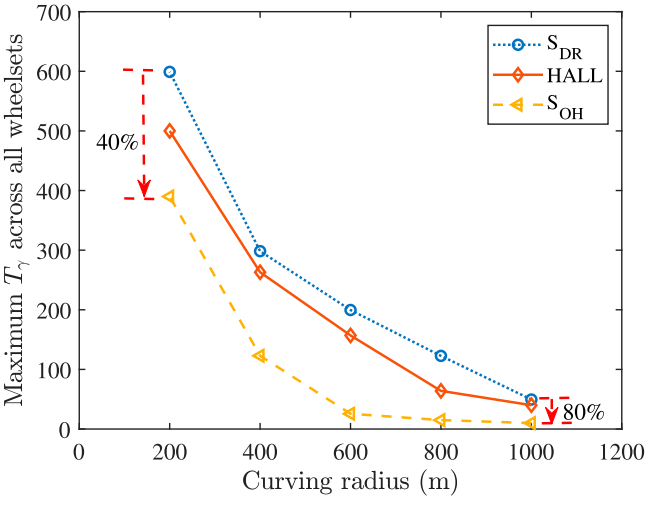

Figure 7. The maximum T_γ comparison among S_{DR}, the HALL® and the S_{OH} with curving radius from 200 m to 1000 m.

is defined as the relative displacement between the wheelset and the bogie. The suspension stroke is an important factor to be monitored, as a reduced PYS could thereby lead to a very large suspension stroke. In practice, the size of the trailing arm bush will limit the amount of the stroke. Under certain scenarios, especially during the tight curves, the suspension will reach the maximum travel in the bush and the vehicle curving performance will therefore be limited. In order to provide satisfactory curving performance, enough space should be available in the trailing arm bush to ensure that the suspension does not reach its displacement limit under such severe cases. As a result, any changes to the suspension stroke due to the reduced PYS could directly influence the suspension packaging size and the potential design complexity.

Figure 8(a,b) illustrates the suspension lateral and longitudinal strokes, respectively, when the curve changes from moderate to tight. The strokes for the S_{DR}, the HALL® and the S_{OH} are compared. From these figures, it can be seen that the suspension strokes tend to increase as the curving radius becomes smaller. From Figure 8(a), the suspension lateral stroke for S_{OH} with its much reduced PYS is slightly smaller compared with both default and the HALL® bush. However, the suspension longitudinal strokes for S_{OH}, especially at the tightest-curve case, are significantly larger than those with two conventional configurations. This could be a concern because the larger longitudinal stroke could either increase the design complexity to accommodate such stoke within the existing bush size for vehicle retrofit, or may lead to an increased bush packaging size and therefore will not be suitable for a conventional vehicle bogie.

5. Optimisation with constrained suspension stroke

With the K_x being reduced to zero in S_{OH}, it has been demonstrated that the rail surface damage during curving can be significantly reduced but a large suspension stroke is observed during a tight curve. Such large stroke will affect the physical design complexity

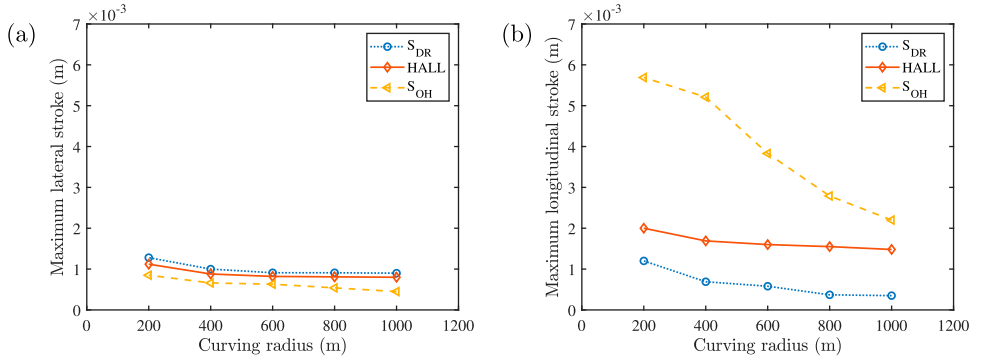

Figure 8. The maximum suspension strokes comparison among S_{DR}, the HALL® and the S_{OH} at (a) lateral direction and (b) longitudinal direction.

and packaging size of the bush. To address this, a more thorough analysis on the trade-off between a constrained suspension stroke and the achievable minimum PYS is presented in this section. Additionally, this section also gives a high-level business case, to estimate the potential cost saving provided by the enhanced trailing arm bush S_{OH} over the traditional S_{DR} and the HALL® considering different suspension stroke limits.

5.1. Trade-off between PYS and suspension stroke

The effects of reducing K_x on suspension strokes for S_{OH} are assessed first. By increasing the K_x from 0 MN/m to 3 MN/m (keeping the other parameters same as the S_{DR}), the resulting lateral and longitudinal suspension strokes are shown in Figure 9. It can be seen that when

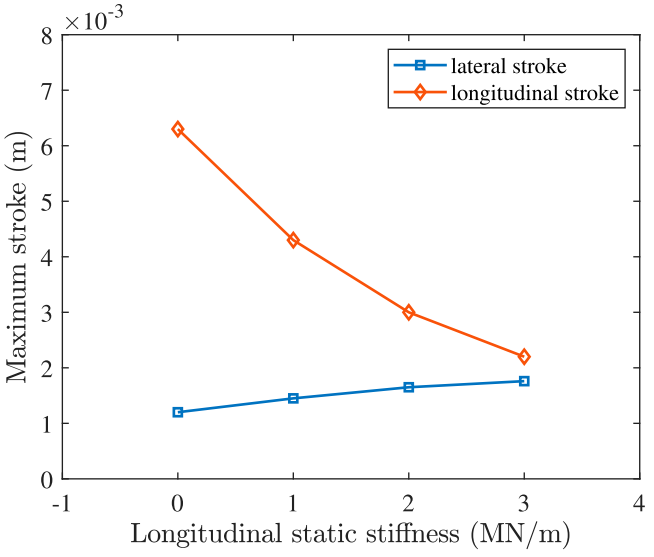

Figure 9. The suspension stroke comparison of S_{OH} with different K_x values during a tight curve (other component values including K_{dx} and C_{dx} have not been changed).

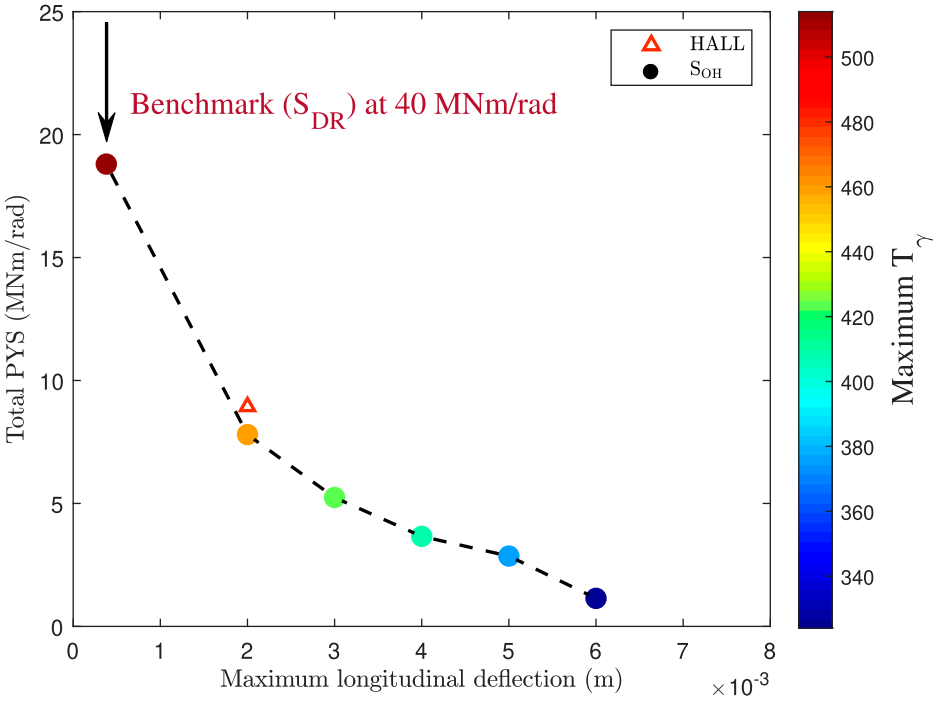

Figure 10. Results for re-optimised trailing arm bush with hydraulic damping integrated considering suspension travel constraints.

increasing the longitudinal static stiffness (K_x), the suspension longitudinal stroke can be significantly reduced, i.e. the maximum suspension stroke is highly dependent on the K_x.

Considering a certain stroke level the suspension can reach to, a new optimisation on the bush is carried out to identify the achievable minimum PYS. In the new optimisation, the ride comfort constraints have been kept same as those stated in Section 3.1, while additional constraint on the suspension longitudinal stroke during the tightest curve has been considered. Table 3 summarised the optimisation results for S_{OH} considering different suspension stroke constraints, as well as the maximum PYS reduction at different cases. Figure 10 has shown the minimum achievable PYS for each stroke constraint as well as the corresponding maximum wheelset T_γ (obtained from 200-metre-radius curve case). A trade-off between the maximum suspension stroke and the achievable minimum PYS can be observed. As the maximum suspension stroke being constrained, the achievable PYS reduction is also limited. For example, the achievable PYS reduction compared with S_{DR} decreases from 97% to 81% if the maximum suspension stroke is limited at from 6 mm to 2 mm. Note that 2 mm is the maximum suspension stroke of the HALL® during 200-metre-radius curve, and a 12.8% PYS reduction can still be achieved with this constrained S_{OH}.

5.2. A high-level business case

In order to provide a more direct understanding of the benefits the enhanced suspension design S_{OH} can bring, a high-level business case is given here. The potential cost saving of

Table 3. Re-optimised suspension parameters with different constraints on the suspension longitudinal stroke.

$Stroke_{max}$ (mm)	K_x (MN/m)	K_{dx} (MN/m)	C_{dx} (kNs/m)	Total PYS (MNm/rad)	PYS reduction (%)
6	0	18.75	6908.9	1.14	97.2
5	0.86	21.26	6753	2.86	92.9
4	1.26	10.30	5781.2	3.66	90.9
3	2.05	21.08	6096.3	5.24	86.9
2	3.33	17.4	7000	7.80	80.5
0.38	8.83	7.83	7000	18.80	53.0

Table 4. Estimated potential savings of optimised configurations in VUC from S_{DR} solution with different suspension stroke limits (4 mm, 6 mm).

Bush type	PYS (%)	VUC (p/vm)	WMM wheelset cost (p/vm)	Annual saving for single vehicle (£K)	Lifetime saving for the fleet (£Mn)
S_{DR}	40.00 (–)	12.09 (–)	2.60 (–)	–	–
HALL®	8.94 (77.7%)	8.82 (27.1%)	2.30 (11.5%)	6.02	24.67
S_{OH}-4 mm	3.66 (90.9%)	7.23 (40.2%)	1.90 (26.9%)	9.38	38.42
S_{OH}-6 mm	1.14 (97.2%)	6.92 (42.8%)	1.70 (34.6%)	10.24	41.94

Note the percentage in bracket shown in the table represents the reduction compared with the default S_{DR} suspension.

new designs over the default bushes is estimated, where the Network Rail Variable Usages Charge (VUC) calculator [26] is applied to obtain the track maintenance cost, while the VTISM – Wheelset Maintenance Model (WMM) calculator [27,28] is applied for wheelset maintenance cost calculation. The VUC calculator is a standard industry approach in UK in calculating the marginal costs to infrastructure from rolling stock, which outputs costs in pence per vehicle mile (p/vm) in the aspects of track, structures, signals and surface damage. The WMM calculator develops a Wheel Profile Damage Model (WPDM) to predict the rate of wear, conicity and rolling contact fatigue (RCF) for wheelsets, hence predicts wheelset maintenance cost in addition to VUC. In this work, the Mark 4 vehicle is simulated to run through a representative mix of track radius with different suspension configurations. The obtained corresponding wheelset T_γ profiles – the key characteristics of vehicles that influence damage to infrastructure and wheelsets, are calculated to determine the wheel–rail surface damage, hence the total maintenance costs. Note that the difference in VUC for vehicles with different suspension configurations only attribute to the difference in surface damage, the costs in track, structures and signals are kept as the default, as these factors are not determined by the wheelset T_γ profiles. The VUC and WMM calculation results have been summarised in Table 4. As shown in the third and fourth column of this table, regarding the S_{DR} as the benchmark, the HALL® bush on Mark 4 vehicle brings 27% VUC reduction and 12% WMM reduction. If a 6 mm suspension stroke constraint is applied, the optimised hydraulic suspension configuration S_{OH} ($K_x = 0$ MN/m) can provide a 43% VUC reduction and 35% WMM reduction. Moreover, if a smaller suspension stroke, 4 mm is allowed, the VUC and WMM cost can be respectively reduced by 35% and 27% by the optimised S_{OH} configuration.

Further investigation on the lifetime cost saving of the Mark 4 fleet has also been carried out in this research. Based on the data given in [29], the total vehicle miles from all the Mark 4 Coaches operating on the East Coast Main Line (ECML) can be determined. It is important to note that the model was based on data in 2019 and therefore before the

replacement of many of the Mark 4's by the class 800 trains (Azumas). Based on these data, there were 302 Mark 4 Coaches running on the ECML with the estimated average of 169 thousand miles each year. With these figures, it can be estimated that the total coverage of the Mark 4 fleet on the ECML is in the region of 50 million vehicle miles per year. Moreover, a 20 years lifetime for vehicles is assumed, with a discounting factor of 3.5% applied as per UK Transport Appraisal Guidance, to estimate the lifetime vehicle miles, so as the lifetime cost saving.

It should also be noted that apart from the reduction in VUC and WMM costs, there are many factors affecting the potential whole life benefit of the enhanced trailing arm bush, such as development, production, fitment, maintenance cost of the enhanced bush designs, as well as the life-span consideration. For the business case of this work, those factors are assumed to be the same, while only the VUC and WMM reductions are estimated for different suspension configurations. As shown in Table 4, it has been calculated that the hydraulic-damping-integrated bush with stroke limits of 4 mm and 6 mm can provide the lifetime saving for the whole Mark 4 fleet of approximately £38 million and £42 million, respectively (the HALL® bush saves approximately £25 m). The results have proved that, with a larger allowable suspension stroke during curving, more lifetime cost saving can be achieved. Note that while the corresponding physical design complexity to accommodate such large suspension stroke could be increased, the additional manufacturing cost should be moderate considering the fact only conventional components (orifices, fluid tubes) are needed.

6. Conclusion

This work fully explored the potential of integrating hydraulic damping into bogie primary suspension on rail surface reduction, as well as the trade-off between the achievable damage reduction and the allowable suspension stroke. It has been found that with hydraulic damping integrated, a 97% vehicle PYS reduction can be achieved with the optimised primary suspension for Mark 4 Coach. This will result in 43% VUC reduction and 35% WMM reduction over the default rubber bush. The vehicle wheelset and suspension performance provided with the optimal suspension are found to be within acceptable ranges, except the increased suspension stroke during tight curves. This could be a concern as for vehicle retrofit, the existing suspension size will limit the amount of the stroke, therefore limiting the vehicle curving performance and surface damage reduction. To address this matter, the optimisation on hydraulic-damping-integrated suspension with different stroke constraints is carried out. The results demonstrated a trade-off between the surface damage reduction and the allowable suspension stroke level. In addition, this paper provides the total lifetime cost saving for the Mark 4 fleet due to the introduction of optimised suspension designs compared with the conventional configuration. It has been shown that with the suspension stroke limit set as 4 mm and 6 mm, the lifetime cost saved by the optimised designs over the default case can potentially be £38 million and £42 million, respectively. This paper therefore could give engineers a guideline on primary suspension design with hydraulic damping integrated, and provide motivation to conduct detailed engineering design studies to further examine the trade-off in terms of design complexity caused and financial benefits achieved.

Notes

1. '45t' and '40yaw' stand for the vehicle total weight of 45 tonnes and total PYS of 40 MNm/rad, respectively.
2. The RMS of carbody lateral acceleration is calculated by taking average values of the RMS lateral accelerations measured at floor level above the centre of the two bogies.

Disclosure statement

No potential conflict of interest was reported by the author(s).

Funding

The authors would like to acknowledge the Rail Safety and Standards Board (RSSB) for funding this research and an EPSRC Fellowship (Grant Number: EP/T016485/1) for the support.

ORCID

Y. Li http://orcid.org/0000-0002-3897-9942

References

[1] Ye Y, Sun Y, Dongfang S, et al. Optimizing wheel profiles and suspensions for railway vehicles operating on specific lines to reduce wheel wear: a case study. Multibody Syst Dyn. 2020;51:91–122.
[2] Wickens AH. Railway vehicles with generic bogies capable of perfect steering. Vehicle System Dynamics. 1996;25(6):389–412.
[3] Mazzola L, Alfi S, Bruni S. A method to optimize stability and wheel wear in railway bogies. International Journal of Railway. 2010;3(3):95–105.
[4] He Y, Mcphee J. Optimization of curving performance of rail vehicles. Vehicle System Dynamics. 2005;43(12):895–923.
[5] Liu X, Goodall R, Iwnicki S. Active control of independently-rotating wheels with gyroscopes and tachometers-simple solutions for perfect curving and high stability performance. Vehicle System Dynamics. 2020;59:1719–1734.
[6] Goodall R, Mei TX. Mechatronic strategies for controlling railway wheelsets with independently rotating wheels. 2001 IEEE/ASME International Conference on Advanced Intelligent Mechatronics. Proceedings (Cat. No. 01TH8556); IEEE; 2001, Vol. 1, p. 225–230.
[7] Mei TX, Goodall R. Practical strategies for controlling railway wheelsets independently rotating wheels. J Dyn Sys, Meas, Control. 2003;125(3):354–360.
[8] Lewis TD, Li Y, Tucker GJ, et al. Improving the track friendliness of a four-axle railway vehicle using an inertance-integrated lateral primary suspension. Vehicle System Dynamics. 2019;59:115–134.
[9] Jiang JZ, Mei TX, Smith MC. Curving performance for railway vehicles with advanced passive suspensions. 23rd International Symposium on Dynamics of Vehicle on Road and Tracks, IAVSD; 2013.
[10] Lewis TD, Jiang JZ, Neild SA, et al. Using an inerter-based suspension to improve both passenger comfort and track wear in railway vehicles. Vehicle System Dynamics. 2020;58(3):472–493.
[11] Fergusson SN, Fröhling RD, Klopper H. Minimising wheel wear by optimising the primary suspension stiffness and centre plate friction of self-steering bogies. Vehicle System Dynamics. 2008;46(S1):457–468.
[12] Wickens AH. The dynamics of railway vehicles on straight track: fundamental considerations of lateral stability. I.MechE, 1965.
[13] Mousavi-Bideleh SM, Berbyuk V. Multiobjective optimisation of bogie suspension to boost speed on curves. Vehicle System Dynamics. 2016;54(1):58–85.

[14] Simson SA, Cole C. Simulation of curving at low speed under high traction for passive steering hauling locomotives. Vehicle System Dynamics. 2008;46(12):1107–1121.
[15] Grassie SL, Elkins JA. Tractive effort, curving and surface damage of rails: part 1. Forces exerted on the rails. Wear. 2005;258(7–8):1235–1244.
[16] Johnsson A, Berbyuk V, Enelund M. Pareto optimisation of railway bogie suspension damping to enhance safety and comfort. Vehicle System Dynamics. 2012;50(9):1379–1407.
[17] Ma T, Liu Y, Qiao X, et al. Fluid-structure-interaction modeling and dynamic behavior analysis for hydrobushing of suspension. Zhongguo Jixie Gongcheng(China Mechanical Engineering). 2013;24(7):857–861.
[18] Eickhoff BM, Evans JR, Minnis AJ. A review of modelling methods for railway vehicle suspension components. Vehicle System Dynamics. 1995;24(6–7):469–496.
[19] Evans JR. The modelling of railway passenger vehicles. Vehicle System Dynamics. 1992;20(supp1):144–156.
[20] Evans JR. Application of the hall hydraulic radial arm bush to a 200 km/h inter-city coach. International Symposium on Dynamics of Vehicle on Road and Tracks, IAVSD; 2011.
[21] Nishimura K, Perkins NC, Zhang W. Suspension dynamics and design optimization of a high speed railway vehicle. ASME/IEEE Joint Rail Conference. 2004;41634:129–139.
[22] Stage 2 development of the Vehicle Track Interaction Strategic Model (T792). Available from: https://www.rssb.co.uk/research-catalogue/CatalogueItem/T792.
[23] BS EN 15302:2021. Railway applications – Wheel-rail contact geometry parameters – Definitions and methods for evaluation.
[24] Swift SJ, Smith MC, Glover AR, et al. Design and modelling of a fluid inerter. Int J Control. 2013;86(11):2035–2051.
[25] Burstow M. Whole Life Rail Model Application and Development for RSSB –Development of an RCF Damage Parameter, AEATR report, (AEATRES-2003–2832 Issue 1, October 2003).
[26] Network Rail VUC calculator. Available from: https://www.networkrail.co.uk/industry-andcommercial/information-for-operators/cp6-access-charges-2.
[27] Gray P. Stage 2 development of the Vehicle Track Interaction Strategic Model (T792). SPARK report, 2014.
[28] Bevan A, Molyneux-Berry P, Eickhoff B, et al. Development and validation of a wheel wear and rolling contact fatigue damage model. Wear. 2013;307(1–2):100–111.
[29] Kent S, Iwnicki S, Houghton T. Options for Traction Energy Decarbonisation in Rail: Options Evaluation. SPARK report, 2019.
[30] Mousavi Bideleh SM, Berbyuk V, Persson R. Wear/comfort Pareto optimisation of bogie suspension. Vehicle System Dynamics. 2016;54(8):1053–1076.

Appendices

Appendix 1: Conicity distribution for P8 wheels and CEN60E2 rail

Rail Standard and Safety Board (RSSB) project T889 included an exercise to measure the worn shape of 400 in-service passenger vehicle P8 wheel profiles. Figure A1 shows the spread of equivalent conicities of those wheels, when combined with a new CEN60E2 rail profile (calculated using the VAMPIRE® contact data generation programme). As shown, there are equivalent conicities up to just under 0.6. The equivalent conicities used in simulations for this paper have been chosen to broadly cover the range shown in this sample. Note that in practice worn rail shape and gauge variation also has an influence on equivalent conicity and that is not considered in the distribution presented in Figure A1.

Wheel-Rail tread and flange contact

Figure A2 shows an example of the tread and flange wheel–rail contact. CL/CR is the wheel–rail creep force at the left/right tread contact point and CF is the wheel–rail creep force at the (left or right) flange contact point. During tight curve scenarios, a large wheelset lateral displacement and

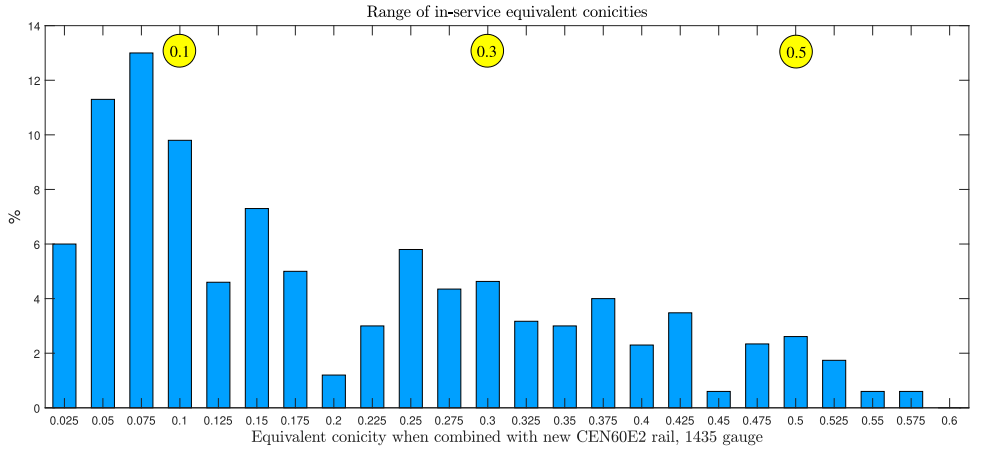

Figure A1. Equivalent conicities from worn wheel combined with new CEN60E2 rail.

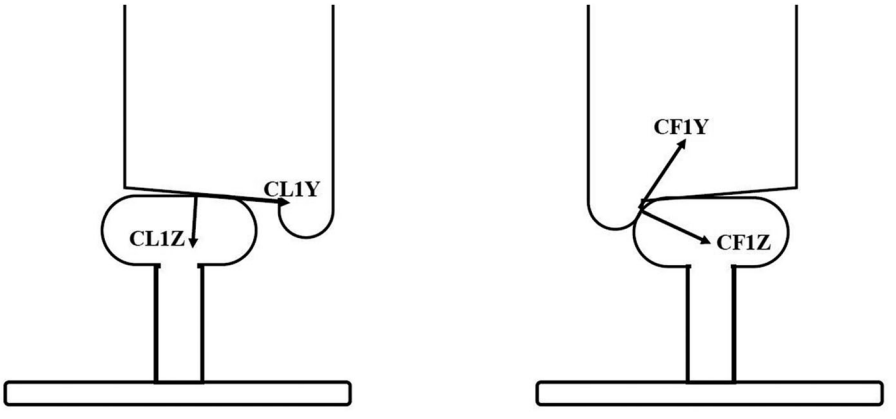

Figure A2. Equivalent conicities from worn wheel combined with new CEN60E2 rail.

angle of attack can lead to a wheel–rail flange contact, resulting in a large wheelset T_γ and hence causing wear.